Alexandria Engineering Journal (2020) 59, 3091–3104

HOSTED BY

Alexandria University

Alexandria Engineering Journal

www.elsevier.com/locate/aej
www.sciencedirect.com

Analysis of a rectangular prism *n*-units RLC fractional-order circuit network

Liping Chen [a,*], Xiaobo Wu [a], Linpeng Xu [a], António M. Lopes [b], J.A. Tenreiro Machado [c], Ranchao Wu [d], Suoliang Ge [a]

[a] *School of Electrical Engineering and Automation, Hefei University of Technology, Hefei 230009, China*
[b] *UISPA–LAETA/INEGI, Faculty of Engineering, University of Porto, Rua Dr. Roberto Frias, 4200-465 Porto, Portugal*
[c] *Institute of Engineering, Polytechnic of Porto, Department of Electrical Engineering, R. Dr. António Bernardino de Almeida, 431, 4249-015 Porto, Portugal*
[d] *School of Mathematics, Anhui University, Hefei 230039, China*

Received 22 October 2019; revised 28 May 2020; accepted 22 June 2020
Available online 7 July 2020

KEYWORDS

Fractional-order circuit networks;
Impedance characteristics;
Phase characteristics

Abstract It was demonstrated recently that ideal capacitors can not exist physically and that the behavior of real-world inductors and capacitors is characterized by fractional-order (FO) models. Therefore, the modeling and analysis of FO electrical circuit networks (FO-ECN) has gained considerable interest. This paper introduces the basic principles of a class of rectangular prism *n*-units ($\diamondsuit \times n$) RLC FO-ECN, including the mathematical modeling and the analysis of the impedance magnitude and phase. Three general formulas of the equivalent impedance between two nodes of the FO-ECN are obtained by the matrix transform method. The relationship between the impedance and the FO-ECN parameters, including the capacitance, inductance, number of circuit units and FO are investigated. Numerical simulations reveal dynamical phenomena not exhibited by ordinary ECN.

1. Introduction

The fundamental concepts of fractional calculus (FC) were introduced three centuries ago. However, the application of FC to real-world problems is just a few decades old. The tools of FC have several advantages for describing systems with hereditary and memory properties [1–22]. Recently, researches showed that real inductors and capacitors exhibit fractional-order (FO) behavior [23–28] and introduced FO models for describing electrical devices [29–37]. In fact, inductors and capacitors have a fractional nature. Circuit models with FO inductors and capacitors can describe circuit characteristics more accurately than standard ones, allowing a high flexibility in matching real-world experimental measurements. Semary et al. [33] proposed the realization of a FO capacitor using passive symmetric networks. Machado and Galhano [38] studied the skin effect and developed a new method for implementing FO inductive elements. Jiang and Zhang [34] discussed the realization of a high-power fractional capacitor of order $1 < \alpha < 2$. Tsirimokou et al. [35] addressed the experimental

* Corresponding author.
E-mail address: lip_chenhut@126.com (L. Chen).
Peer review under responsibility of Faculty of Engineering, Alexandria University.

https://doi.org/10.1016/j.aej.2020.06.042

verification of on-chip CMOS FO capacitor emulators. Tripathy et al. [36] presented the hardware realization and performance analysis of fractional inductors of order $0 < \alpha < 2$.

Electrical circuit networks (ECN) consist on a set of electrical components connected to each other, that are used to transmit, transform, process and store electrical energy or signals. The ECN modeling and analysis has been an important research topic in the last few years. The stability [39], sensitivity [40], passivity [41] and impedance calculation are fundamental problems in the study of ECN. On the other hand, considerable efforts have been devoted to the study of infinite ECN composed entirely of resistors or capacitors. Owaidat et al. [42] adopted the lattice Green function to calculate the efective resistance between any two nodes of a resistive ECN when two additional resistances are introduced. Asad [43] considered the equivalent capacitance between two adjacent nodes in an infinite dimensional capacitive ECN composed of identical capacitors. Hijjawi et al. [44] applied the lattice Green function to calculate the resistance between two arbitrary nodes of a ECN of resistors when the network is perturbed with the inclusion of an extra resistor between two arbitrary nodes. In spite of these advances, the modeling and analysis of ECN has been mostly based on the concept of integer order inductance and capacitance. Therefore, often a simple integer-order model is not accurate enough and does not reflect the essential characteristics of the ECN. Despite the research carried out on ECN, the study of the impedance characteristics of multiple-component ECN, and the study of FO-ECN, have been somewhat overlooked. The FO characteristics of inductance and capacitance not only will directly affect the performance of the whole ECN, but also will bring flexibility to the ECN design. With the FO characteristics of actual inductance and capacitance in mind, FO-ECN are presently receiving great attention. For examples, Chen et al. [45] introduced the fundamentals of a $L_\beta C_\alpha$ infinite rectangle FO-ECN and discussed its relevance and symmetry properties. Zheng et al. [46] analyzed a $L_\beta C_\alpha$ FO-ECN filter. Ün [47] proposed a $2 \times n$ FO-ECN and calculated its equivalent impedances based on the mesh current method. Zhou et al. designed a three-dimensional [48] and a multifunctional n-step honeycomb RLC FO-ECN [49] and investigated their impedance characteristics. In this paper, a novel rectangular prism n-units ($\diamondsuit \times n$) RLC FO-ECN is introduced and its impedance (magnitude and phase) characteristics are analyzed. This article aims to study phenomena that classic ECN do not exhibit. The contributions of the paper include (i) the mathematical modeling of a class of $\diamondsuit \times n$ FO-ECN with multiple-components, and (ii) the determination of the impedance magnitude between two FO-ECN nodes for three different cases, based on FC theory and the matrix transformation method. The effect of six system parameters (number of circuit units (n), fractional order (α, β), capacitance (C), inductance (L), and resistance (R)) on the impedance magnitude characteristics between three different nodes are systematically studied. Moreover, the impedance phase characteristics in two typical situations are analyzed and compared. The relationship between the impedance phase and the order is also illustrated.

The organization of the paper is as follows. Section 2 introduces the necessary definitions and the model of the $\diamondsuit \times n$ RLC FO-ECN. Section 3 derives general formulas of the impedance between two FO-ECN points, using the matrix transform method for three cases. Section 4 analyzes the impedance magnitude characteristics. Section 5 performs the numerical verification and analyses of the accuracy of the method. Section 6 investigates the impedance phase characteristics. Section 7 concludes the paper.

2. Preliminaries and model description

Let us consider a function $x(t)$, where t denotes time. The FO derivative of $x(t)$ can be calculated according to several definitions. The three more common are the Riemann–Liouville (RL), Grünwald-Letnikov (GL) and Caputo (C), given as follows.

Definition 1 [4]. The RL derivative of FO α of $x(t)$ is:

$$ {}_aD_t^\alpha f(t) = \frac{1}{\Gamma(n-\alpha)} \frac{d^n}{dt^n} \int_a^t \frac{f(\tau)}{(t-\tau)^{\alpha-n+1}} d\tau, $$

Definition 2 [4]. The GL derivative of FO α of $x(t)$ is:

$$ {}_aD_t^\alpha f(t) = \lim_{h\to 0} \left(\frac{1}{h^\alpha}\right) \sum_{j=0}^{[(t-\alpha)/h]} (-1)^j \binom{\alpha}{j} f(t-jh), $$

Definition 3 [4]. The Caputo derivative of FO α of $x(t)$ is:

$$ {}_CD_{t_0,t}^\alpha x(t) = \frac{1}{\Gamma(n-\alpha)} \int_{t_0}^t (t-\tau)^{n-\alpha-1} x^{(n)}(\tau) d\tau, $$

where $n-1 < \alpha < n$, $n \in \mathbb{N}$ and $\Gamma(s) = \int_0^\infty t^{s-1} e^{-t} dt$ is the Gamma function.

The inductors and capacitors are crucial elements in integrated circuits and are used extensively in many systems. Recently, several researches showed that the dielectric materials exhibit FO behavior and that an ideal capacitor is not physically realizable. Moreover, real-world inductors and capacitors exhibit FO dynamics [38]. Their impedances are given in [50] andthe mathematical description can be found in the Appendix A. Hereafter, in order to have well understood physical meaning of the initial conditions, the Caputo FO derivative is considered. The fractional models of the inductor and the capacitor can be written as:

$$ \begin{aligned} Z_L &= \omega^\beta L \cos\left(\tfrac{\beta\pi}{2}\right) + j\omega^\beta L \sin\left(\tfrac{\beta\pi}{2}\right), \\ Z_C &= \frac{\cos\left(\frac{\omega\pi}{2}\right)}{\omega^\alpha C} - j\frac{\sin\left(\frac{\omega\pi}{2}\right)}{\omega^\alpha C}, \end{aligned} $$

where the constants L and C represent the inductance and capacitance, while β and α denote the FO of the inductor and capacitor, respectively.

Herein, a class of $\diamondsuit \times n$ RLC FO-ECN is introduced, with the topological structure depicted in Fig. 1. The symbols z_0, z_1 (in blue) and z (in red) denote resistance, FO inductor and FO capacitor, respectively.

3. Equivalent impedance between two different points

3.1. The equivalent impendance between the points *a* and *c*

In this section, we use ECN analysis, matrix transformations and difference equations to derive the impedance between the FO-ECN points a and c.

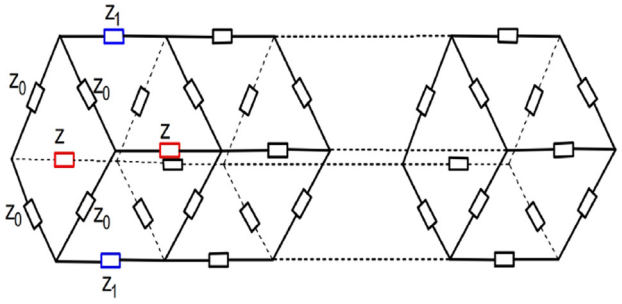

Fig. 1 The topology of the $\diamondsuit \times n$ RLC FO-ECN. The elements z_0, z_1 (in blue) and z (in red) denote the resistance, FO inductor and FO capacitor, respectively.

3.1.1. Establishment of the model

Fig. 2 depicts the sub-network between the points a and c, where the current flows from c to a. The currents in the three rows and in the two columns of the circuit are denoted by I_{ak}, I_{bk} and I_{ck}, and $I_k$and I'_k, respectively.

From Fig. 2, and applying the Kirchhoff's current law (KCL), we obtain the equations relating the currents at points g, h and i, as follows:

$$I_{ak} + 2I_k - I_{ak-1} = 0, \tag{1}$$

$$I_{bk} + I'_k - I_k - I_{bk-1} = 0, \tag{2}$$

$$I_{ck-1} + 2I'_k - I_{ck} = 0. \tag{3}$$

From the Kirchhoff's voltage law (KVL), the equations relating the voltages in the two loops k can be expressed as:

$$I_{bk}z + I_k z_0 - I_{k+1}z_0 - I_{ak}z_1 = 0, \tag{4}$$

$$I'_k z_0 - I'_{k+1}z_0 - I_{ck}z_1 - I_{bk}z = 0. \tag{5}$$

Similarly, the voltage equations in the two loops $k-1$ are:

$$I_{bk-1}z + I_{k-1}z_0 - I_k z_0 - I_{ak-1}z_1 = 0, \tag{6}$$

$$I'_{k-1}z_0 - I'_k z_0 - I_{ck-1}z_1 - I_{bk-1}z = 0. \tag{7}$$

Combining expressions (4)–(7) results in:

$$(2I_k - I_{k+1} - I_{K-1})z_0 + (I_{bk} - I_{bk-1})z + (I_{ak-1} - I_{ak})z_1 = 0, \tag{8}$$

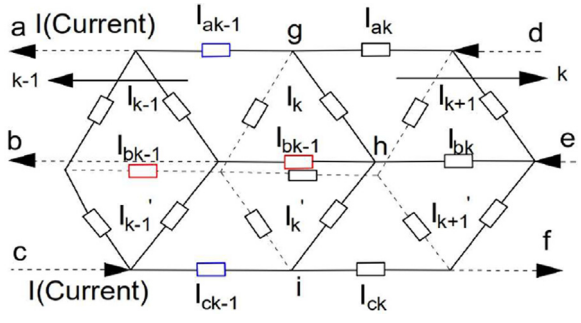

Fig. 2 The sub-network between the points a and c of the $\diamondsuit \times n$ RLC FO-ECN. The elements in blue and red denote the FO inductor and FO capacitor, respectively.

$$(2I'_k - I'_{k+1} - I'_{k-1})z_0 + (I_{ck} - I_{ck-1})z_1 + (I_{bk-1} - I_{bk}) = 0. \tag{9}$$

From (1)–(3), expressions (8) and (9) can be rewritten as follows:

$$(I_{k+1} + I_{k-1})z_0 = (2z_0 + z + 2z_1)I_k - zI'_k, \tag{10}$$

$$(I'_{k+1} + I'_{k-1})z_0 = (2z_0 + z + 2z_1)I'_k - zI_k. \tag{11}$$

Expressions (10) and (11) yield:

$$I_{k+1} + I_{k-1} = (2 + a + 2b)I_k - aI'_k, \tag{12}$$

$$I'_{k+1} + I'_{k-1} = (2 + a + 2b)I'_k - aI_k, \tag{13}$$

where $a = z/z_0$ and $b = z_1/z_0$.

The formulation (12) and (13) can be written in matrix form as:

$$\begin{bmatrix} I_{k+1} \\ I'_{k+1} \end{bmatrix} = \begin{bmatrix} 2+a+2b & -a \\ -a & 2+a+2b \end{bmatrix} \begin{bmatrix} I_k \\ I'_k \end{bmatrix} - \begin{bmatrix} I_{k-1} \\ I'_{k-1} \end{bmatrix}. \tag{14}$$

To solve for I_k and I'_k, we multiply (14) by a second-order matrix $\begin{bmatrix} \lambda_1 & 1 \\ \lambda_2 & 1 \end{bmatrix}$, yielding:

$$\begin{aligned} &\begin{bmatrix} \lambda_1 & 1 \\ \lambda_2 & 1 \end{bmatrix} \begin{bmatrix} I_{k+1} \\ I'_{k+1} \end{bmatrix} = \begin{bmatrix} \lambda_1 & 1 \\ \lambda_2 & 1 \end{bmatrix} \\ \times &\begin{bmatrix} 2+a+2b & -a \\ -a & 2+a+2b \end{bmatrix} \begin{bmatrix} I_k \\ I'_k \end{bmatrix} - \begin{bmatrix} \lambda_1 & 1 \\ \lambda_2 & 1 \end{bmatrix} \begin{bmatrix} I_{k-1} \\ I'_{k-1} \end{bmatrix}. \end{aligned} \tag{15}$$

Assuming that there exist two undefined constants t_1 and t_2, such that:

$$\begin{bmatrix} \lambda_1 & 1 \\ \lambda_2 & 1 \end{bmatrix} \begin{bmatrix} 2+a+2b & -a \\ -a & 2+a+2b \end{bmatrix} = \begin{bmatrix} t_1 & 0 \\ 0 & t_2 \end{bmatrix} \begin{bmatrix} \lambda_1 & 1 \\ \lambda_2 & 1 \end{bmatrix}, \tag{16}$$

then, from (16), we have:

$$\begin{bmatrix} \lambda_1(2+a+2b) - a & -a\lambda_1 + 2 + a + 2b \\ \lambda_2(2+a+2b) - a & -a\lambda_2 + 2 + a + 2b \end{bmatrix} = \begin{bmatrix} t_1\lambda_1 & t_1 \\ t_2\lambda_2 & t_2 \end{bmatrix}, \tag{17}$$

that can be expressed as:

$$\begin{cases} \lambda_i(2+a+2b) - a = t_i\lambda_i \\ -a\lambda_i + 2 + a + 2b = t_i \end{cases}, \tag{18}$$

where $i = 1, 2$.

We obtain two solutions for expression (18), namely:

$$\begin{cases} \lambda_1 &= 1 \\ t_1 &= 2 + 2b \end{cases}, \tag{19a}$$

$$\begin{cases} \lambda_2 &= -1 \\ t_2 &= 2 + 2a + 2b \end{cases}. \tag{19b}$$

Substituting (19) into (15) and (16), expression (15) can be written as:

$$\begin{bmatrix} I'_{k+1} + I_{k+1} \\ I'_{k+1} - I_{k+1} \end{bmatrix} = \begin{bmatrix} t_1 & 0 \\ 0 & t_2 \end{bmatrix} \begin{bmatrix} I'_k + I_k \\ I'_k - I_k \end{bmatrix} - \begin{bmatrix} I'_{k-1} + I_{k-1} \\ I'_{k-1} - I_{k-1} \end{bmatrix}. \tag{20}$$

With the solution method of the second-order linear difference equation, the characteristic equation of (20) is given by:

$$\begin{bmatrix} x^2 \\ y^2 \end{bmatrix} = \begin{bmatrix} t_1 & 0 \\ 0 & t_2 \end{bmatrix} \begin{bmatrix} x \\ y \end{bmatrix} - \begin{bmatrix} 1 \\ 1 \end{bmatrix}. \tag{21}$$

Let p and q (and γ and δ) stand for the two solutions of the Eq. (21) about x (and about y). Therefore, the solutions are given by:

$$\begin{bmatrix} p \\ q \end{bmatrix} = \begin{bmatrix} \frac{1}{2}\left(2+2b+\sqrt{(2+2b)^2-4}\right) \\ \frac{1}{2}\left(2+2b-\sqrt{(2+2b)^2-4}\right) \end{bmatrix}, \tag{22}$$

and

$$\begin{bmatrix} \gamma \\ \delta \end{bmatrix} = \begin{bmatrix} \frac{1}{2}\left(2+2a+2b+\sqrt{(2+2a+2b)^2-4}\right) \\ \frac{1}{2}\left(2+2a+2b-\sqrt{(2+2a+2b)^2-4}\right) \end{bmatrix}. \tag{23}$$

Using $I'_{k+1}+I_{k+1}=x_{k+1}$ and $I'_{k+1}-I_{k+1}=y_{k+1}$, expression (21) can be rewritten as:

$$x_{k+1} = (p+q)x_k - pqx_{k-1}, \tag{24a}$$

$$y_{k+1} = (\gamma+\delta)y_k - \gamma\delta y_{k-1}. \tag{24b}$$

From (24), one can easily obtain:

$$\begin{cases} x_{k+1} - px_k = q^{k-1}(x_2 - px_1) \\ x_{k+1} - qx_k = p^{k-1}(x_2 - qx_1) \end{cases}, \tag{25}$$

$$\begin{cases} y_{k+1} - \gamma x_k = \delta^{k-1}(x_2 - \gamma x_1) \\ y_{k+1} - \delta x_k = \gamma^{k-1}(x_2 - \delta x_1) \end{cases}. \tag{26}$$

Therefore, it follows from (25) and (26) that:

$$\begin{bmatrix} x_k \\ y_k \end{bmatrix} = \begin{bmatrix} \frac{1}{p-q}[(x_2 - qx_1)p^{k-1} - (x_2 - px_1)q^{k-1}] \\ \frac{1}{\gamma-\delta}[(x_2 - \delta x_1)\gamma^{k-1} - (x_2 - \gamma x_1)\delta^{k-1}] \end{bmatrix}, \tag{27}$$

where $k = 3, 4, 5, \cdots$.

Finally, the solutions of the second-order difference Eqs. (14) can be obtained as follows:

$$\begin{aligned} I'_k &= \tfrac{1}{2}(x_k + y_k) \\ &= \tfrac{1}{2}\left(\tfrac{1}{p-q}[(x_2 - qx_1)p^{k-1} - (x_2 - px_1)q^{k-1}\right. \\ &+ \left.\tfrac{1}{\gamma-\delta}[(x_2 - \delta x_1)\gamma^{k-1} - (x_2 - \gamma x_1)\delta^{k-1}]\right), \end{aligned} \tag{28}$$

$$\begin{aligned} I_k &= \tfrac{1}{2}(x_k - y_k) \\ &= \tfrac{1}{2}\left(\tfrac{1}{p-q}[(x_2 - qx_1)p^{k-1} - (x_2 - px_1)q^{k-1}\right. \\ &- \left.\tfrac{1}{\gamma-\delta}[(x_2 - \delta x_1)\gamma^{k-1} - (x_2 - \gamma x_1)\delta^{k-1}]\right). \end{aligned} \tag{29}$$

3.1.2. The law of the boundary current

Fig. 3 depicts the $\diamondsuit \times n$ RLC FO-ECN between the points a and c, with boundary conditions. Exploring the symmetries of the FO-ECN, we verify that $I_k = I'_k$. Therefore, expression (12) can be rewritten as:

$$I_{k+1} = (2+2b)I_k - I_{k-1},$$

and from (30):

$$I_k = \frac{1}{p-q}[(I_2 - qI_1)p^{k-1} - (I_2 - pI_1)q^{k-1}]. \tag{31}$$

Furthermore, we may write:

$$\sum_{i=1}^{n+1} 2I_i = I. \tag{32}$$

Summing the $n+1$ currents in (31) and using (32), it yields:

$$\frac{2}{p-q}\left[(I_2 - qI_1)\frac{1-p^{n+1}}{1-p} - (I_2 - pI_1)\frac{1-q^{n+1}}{1-q}\right] = I. \tag{33}$$

Exploring the FO-ECN symmetry, the equations relating the currents on the left part are:

$$I_{c1} + 2I'_1 = I,\ I_{b1} = 0,\ I_{a1} + 2I_1 = I, \tag{34}$$

and the equation relating the voltages in the first loop, shown in purple in Fig. 3, is:

$$-I_2 z_0 + I_{b1} z + I_1 z_0 - I_{a1} z_1 = 0. \tag{35}$$

Therefore, based on expressions (34) and (35), we have:

$$I_2 = I_1(1+2b) - bI. \tag{36}$$

Since p and q in (22) are the two solutions of the equation about x, expression (36) can be rewritten as:

$$I_2 = I_1(p+q-1) - \frac{I}{2}(p+q-2). \tag{37}$$

Then, substituting (37) into (33) yields:

$$I_1 = \frac{1}{2}\left(1 - \frac{p^n - q^n}{p^{n+1} - q^{n+1}}\right)I. \tag{38}$$

3.1.3. The equivalent impedance between the points a and c

From Fig. 3, the voltage between the points a and c can be expressed by:

$$U_{ac} = I_1 z_0 + I'_1 z_0. \tag{39}$$

Exploring the FO-ECN symmetry, we have the relation $I_1 = I'_1$. Therefore, expression (39) is equivalent to:

$$U_{ac} = 2I_1 z_0. \tag{40}$$

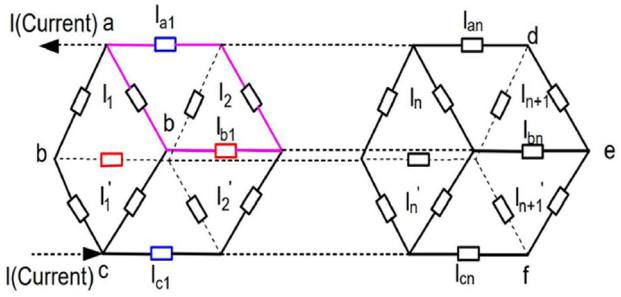

Fig. 3 The diagram of the $\diamondsuit \times n$ RLC FO-ECN between the points a and c, with boundary conditions. The elements in blue and red denote the FO inductor and FO capacitor, respectively. The first loop is shown in purple.

Furthermore, using the Ohm's law, the equivalent impedance between the points a and c is given by:

$$Z_{ac}(n) = \frac{U_{ac}}{I} = 2\frac{I_1}{I} z_0. \tag{41}$$

Hence, combining (38) with (41) yields:

$$Z_{ac}(n) = \left(1 - \frac{p^n - q^n}{p^{n+1} - q^{n+1}}\right) z_0, \tag{42}$$

where $n = 1, 2, 3, \cdots$.

Expression (42) represents the equivalent impedance between the points a and c of the FO-ECN. It should be noted that this impedance is independent of the FO capacitors. Moreover, from (22), it follow that $p > q$ and

$$\lim_{n \to n_0} \left(\frac{q}{p}\right)^n \to 0. \tag{43}$$

Thus, expression (42) can be rewritten as:

$$\lim_{n \to n_0} Z_{ac}(n) = \left(1 - \frac{1}{p}\right) z_0. \tag{44}$$

3.2. The equivalent impedance between the points c and f

In this section the equivalent FO-ECN impedance between the points c and f is calculated.

3.2.1. Establishment of the model

Fig. 4 depicts the $\diamondsuit \times n$ RLC FO-ECN sub-network between the points c and f. Comparing Figs. 4 and 2, we verify that they differ essentially on the direction of the currents. Therefore, the analyses presented in Section 2 can be adopted herein, yielding the difference equations:

$$\begin{bmatrix} I'_{k+1} + I_{k+1} \\ I'_{k+1} - I_{k+1} \end{bmatrix} = \begin{bmatrix} t_1 & 0 \\ 0 & t_2 \end{bmatrix} \begin{bmatrix} I'_k + I_k \\ I'_k - I_k \end{bmatrix} - \begin{bmatrix} I'_{k-1} + I_{k-1} \\ I'_{k-1} - I_{k-1} \end{bmatrix}. \tag{45}$$

Expressions (45) and (20) are identical, meaning that despite representing different cases, both sub-networks have the same model. Therefore, the solutions of expression (45) are those in (28) and (29).

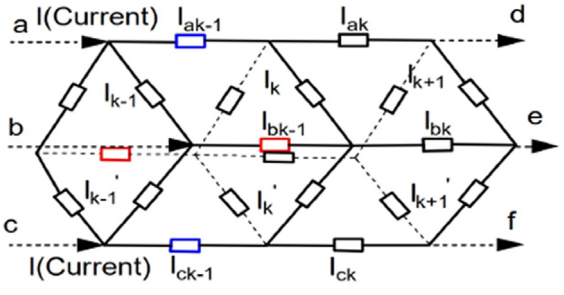

Fig. 4 The sub-network between the points c and f of the $\diamondsuit \times n$ RLC FO-ECN. The elements in blue and red denote the FO inductor and FO capacitor, respectively.

3.2.2. The law of boundary current

Fig. 5 represents the $\diamondsuit \times n$ RLC FO-ECN between the points c and f, with boundary conditions. Based on the KCL, the boundary current is given by:

$$\begin{bmatrix} I_2 \\ I'_2 \end{bmatrix} = \begin{bmatrix} 1 + a + b & -a \\ -a & 1 + a + b \end{bmatrix} \begin{bmatrix} I_1 \\ I'_1 \end{bmatrix} - \begin{bmatrix} 0 \\ bI \end{bmatrix}. \tag{46}$$

Since $x_k = I'_k + I_k$ and $y_k = I'_k - I_k$, expression (46) becomes:

$$\begin{bmatrix} x_2 \\ y_2 \end{bmatrix} = \begin{bmatrix} (p + q - 1)x_1 \\ (\gamma + \delta - 1)y_1 \end{bmatrix} + \begin{bmatrix} -bI \\ -bI \end{bmatrix}. \tag{47}$$

Furthermore, according to the direction of the currents, we obtain:

$$\begin{cases} \sum_{i=1}^{n+1} I'_i = 0, \\ \sum_{i=1}^{n+1} I_i = 0. \end{cases} \tag{48}$$

Hence, taking the sum of the variables x_k and y_k, for $k = 1, \cdots, n$, and using expression (48), it results:

$$\begin{bmatrix} \frac{1}{p-q}\left[(x_2 - qx_1)\frac{1-p^{n+1}}{1-p} - (x_2 - px_1)\frac{1-q^{n+1}}{1-q}\right] \\ \frac{1}{\gamma-\delta}\left[(x_2 - \delta x_1)\frac{1-\gamma^{n+1}}{1-\gamma} - (x_2 - \gamma x_1)\frac{1-\delta^{n+1}}{1-\delta}\right] \end{bmatrix} = \begin{bmatrix} 0 \\ 0 \end{bmatrix}. \tag{49}$$

In view of (47) and (49), the formula of the boundary current is:

$$\begin{bmatrix} x_1 \\ y_1 \end{bmatrix} = \begin{bmatrix} \frac{1}{2}\left(1 - \frac{(p^n - q^n) + (p-q)}{p^{n+1} - q^{n+1}}\right) \\ \frac{b}{2a+2b}\left(1 + \frac{(\delta^n - \gamma^n) + (\delta - \gamma)}{\gamma^{n+1} - \delta^{n+1}}\right) \end{bmatrix} I. \tag{50}$$

3.2.3. The equivalent impedance between the points c and f

In Fig. 5 we observe that it is easily to derive the voltage equations between the points c and f, that yield:

$$\begin{cases} U_{cf} = \sum_{i=1}^{n} I_{ai} z_1 + (I_1 + I'_1 - I_{n+1} - I'_{n+1}) z_0, \\ U_{cf} = \sum_{i=1}^{n} I_{bi} z + (I'_1 - I'_{n+1}) z_0, \\ U_{cf} = \sum_{i=1}^{n} I_{ci} z_1. \end{cases} \tag{51}$$

Adding the three equations in (51) results:

$$3U_{cf} = \sum_{i=1}^{n} (I_{ai} z_1 + I_{bi} z + I_{ci} z_1) + (2I'_1 + I_1 - 2I'_{n+1} - I_{n+1}) z_0. \tag{52}$$

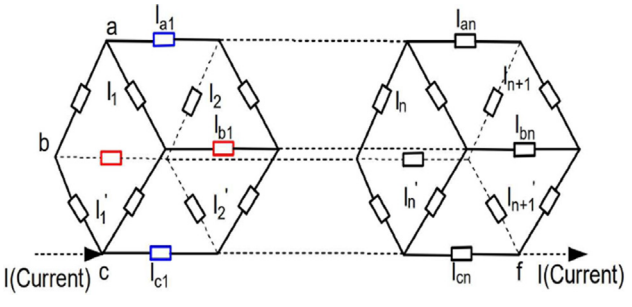

Fig. 5 The diagram of the $\diamondsuit \times n$ RLC FO-ECN between the points c and f, with boundary conditions. The elements in blue and red denote the FO inductor and FO capacitor, respectively.

Moreover, exploring the FO-ECN symmetries, we obtain:

$$\begin{cases} I'_{n+1} = -I'_1, \\ I_{n+1} = -I_1, \\ \sum_{i=1}^{n}(I_{ai} + 2I_{bi} + I_{ci}) = nI. \end{cases} \tag{53}$$

According to the KVL, we also have:

$$\begin{cases} \sum_{i=1}^{n} I_{bi} = \frac{1}{z}\left(z_1 \sum_{i=1}^{n} I_{ai} + 2z_0 I_1\right), \\ \sum_{i=1}^{n} I_{ci} = \frac{1}{z_1}\left(z_1 \sum_{i=1}^{n} I_{ai} + 2z_0\left(I_1 + I'_1\right)\right) \end{cases}. \tag{54}$$

Combining expressions (52) and (54) with (53) yields:

$$3U_{cf} = 3z_1 \sum_{i=1}^{n} I_{ai} + 6z_0(I_1 + I'_1). \tag{55}$$

Similarly, substituting (54) into (53) results in:

$$\sum_{i=1}^{n} I_{ai} = \frac{\frac{nIz}{z_1} - \left(\frac{2zz_0}{z_1^2} + \frac{4z_0}{z_1}\right) I_1 - \frac{2zz_0}{z_1^2} I'_1}{2d+2}. \tag{56}$$

Therefore, it follows from (55) and (56) that:

$$3U_{cf} = \frac{3nz}{2d+2} I + \left[\left(6 - \frac{6+3d}{d+1}\right) I_1 + \left(6 - \frac{3d}{d+1}\right) I'_1\right] z_0, \tag{57}$$

where $I_1 = \frac{x_1 - y_1}{2}$ and $I'_1 = \frac{x_1 + y_1}{2}$.

Obviously, expression (57) can be rewritten as:

$$\begin{aligned} U_{cf} = [&\frac{nz}{2d+2} + \frac{1}{2}\left[1 - \frac{(p^n - q^n) + (p - q)}{p^{n+1} - q^{n+1}}\right] z_0 \\ &+ \frac{1}{2(d+1)^2}\left[1 + \frac{(\delta^n - \gamma^n) + (\delta - \gamma)}{\gamma^{n+1} - \delta^{n+1}}\right] z_0] I. \end{aligned} \tag{58}$$

Therefore, the equivalent impedance between the points c and f is given by:

$$\begin{aligned} Z_{cf}(n) = &\frac{nz}{2d+2} + \frac{1}{2}\left[1 - \frac{(p^n - q^n) + (p - q)}{p^{n+1} - q^{n+1}}\right] z_0 \\ &+ \frac{1}{2(d+1)^2}\left[1 + \frac{(\delta^n - \gamma^n) + (\delta - \gamma)}{\gamma^{n+1} - \delta^{n+1}}\right] z_0, \end{aligned} \tag{59}$$

where $n = 1, 2, 3, \cdots$.

3.3. The equivalent impedance between the points c and d

3.3.1. Establishment of model

From Fig. 4 and the results obtained previously, the difference equations model for the impedance between the points c and d is as follow:

$$\begin{bmatrix} I'_{k+1} + I_{k+1} \\ I'_{k+1} - I_{k+1} \end{bmatrix} = \begin{bmatrix} t_1 & 0 \\ 0 & t_2 \end{bmatrix} \begin{bmatrix} I'_k + I_k \\ I'_k - I_k \end{bmatrix} - \begin{bmatrix} I'_{k-1} + I_{k-1} \\ I'_{k-1} - I_{k-1} \end{bmatrix}. \tag{60}$$

Therefore, the solutions of (60) are those of the model (20), as given by expressions (28) and (29).

3.3.2. The law of boundary current

Fig. 6 depicts the $\diamondsuit \times n$ RLC FO-ECN between the points c and d, with boundary conditions. The boundary current can be expressed as

$$\begin{bmatrix} x_2 \\ y_2 \end{bmatrix} = \begin{bmatrix} (p + q - 1)x_1 \\ (\gamma + \delta - 1)y_1 \end{bmatrix} + \begin{bmatrix} -bI \\ -bI \end{bmatrix}. \tag{61}$$

Furthermore, from Figs. 4 and 6 and considering the directions of the currents, we have:

$$\begin{cases} \sum_{i=1}^{n+1} I'_i = \frac{1}{2} I, \\ \sum_{i=1}^{n+1} I_i = \frac{1}{2} I. \end{cases} \tag{62}$$

Hence, summing x_k and $y_k, k = 1, \ldots, n$, and in view of (62), it yields:

$$\begin{bmatrix} \frac{1}{p-q}\left[(x_2 - qx_1)\frac{1-p^{n+1}}{1-p} - (x_2 - px_1)\frac{1-q^{n+1}}{1-q}\right] \\ \frac{1}{\gamma-\delta}\left[(x_2 - \delta x_1)\frac{1-\gamma^{n+1}}{1-\gamma} - (x_2 - \gamma x_1)\frac{1-\delta^{n+1}}{1-\delta}\right] \end{bmatrix} = \begin{bmatrix} I \\ 0 \end{bmatrix}. \tag{63}$$

Substituting of (63) into (62) gives:

$$\begin{bmatrix} x_1 \\ y_1 \end{bmatrix} = \begin{bmatrix} \frac{1}{2}\left(1 + \frac{(p-q) - (p^n - q^n)}{p^{n+1} - q^{n+1}}\right) \\ \frac{b}{2a+2b}\left(1 + \frac{(\delta^n - \gamma^n) + (\delta - \gamma)}{\gamma^{n+1} - \delta^{n+1}}\right) \end{bmatrix} I. \tag{64}$$

3.3.3. The equivalent impedance between the points c and d

From Fig. 6, we can obtain the voltage equations between the two points c and d as follows:

$$\begin{cases} U_{cd} = \sum_{i=1}^{n} I_{ai} z_1 + (I_1 + I'_1) z_0, \\ U_{cd} = \sum_{i=1}^{n} I_{bi} z + (I'_1 - I_{n+1}) z_0, \\ U_{cd} = \sum_{i=1}^{n} I_{ci} z_1 + (I'_{n+1} - I'_{n+1}) z_0. \end{cases} \tag{65}$$

Adding the three equations in (65) we obtain:

$$3U_{cd} = \sum_{i=1}^{n} (I_{ai} z_1 + I_{bi} z + I_{ci} z_1) + (2I'_1 + I_1 + 2I_{n+1} + I'_{n+1}) z_0. \tag{66}$$

Exploring the FO-ECN symmetries we have:

$$\begin{cases} I'_{n+1} = I_1, \\ I_{n+1} = I'_1, \\ \sum_{i=1}^{n}(I_{ai} + 2I_{bi} + I_{ci}) = nI. \end{cases} \tag{67}$$

Therefore, adopting the method of analysis presented in the determination of the impedance between the points c and f, from (65)–(67), the equivalent impedance between the points c and d can be given by:

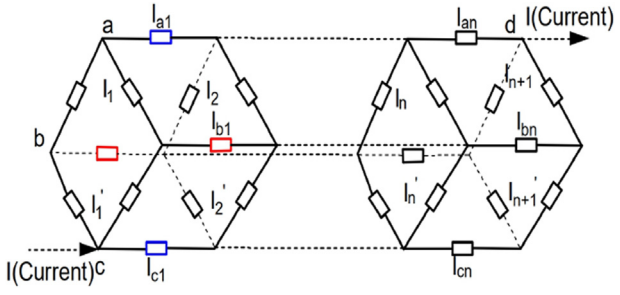

Fig. 6 The diagram of the $\diamondsuit \times n$ RLC FO-ECN between the points c and d, with boundary conditions. The elements in blue and red denote the FO inductor and FO capacitor, respectively.

$$Z_{cd}(n) = \frac{nz}{2d+2} + \frac{1}{2}\left[1 + \frac{(p-q)-(p^n-q^n)}{p^{n+1}-q^{n+1}}\right] z_0 + \frac{1}{3(d+1)^2}\left[1 + \frac{(\delta^n-\gamma^n)+(\delta-\gamma)}{\gamma^{n+1}-\delta^{n+1}}\right] z_0, \quad (68)$$

where $n = 1, 2, 3, \cdots$.

4. Magnitude characteristics of the impedance

In this subsection, we analyze numerically the magnitude characteristics of the impedance of the FO-ECN between the points a and c, and c and f. We use the three impedance formulas (42) and (59) obtained in Section 3 to carry out simulation experiments. Several sets of parameter values $(R, L, C, \alpha, \beta, n, \omega)$ are adopted to obtain simulation results that are illustrative. The software MATLAB R2014b was used in all experiments.

4.1. Magnitude characteristics of the impedance between the points a and c

In the follow-up all variables are expressed in the figures captions. We start by choosing $R = 0.1, L = 0.01$ and $\omega = 300$, while varying n and β. Fig. 7 depicts the impedance magnitude, Z, versus $n \in [0, 50]$ and $\beta \in \{0.1, 0.4, 0.7, 1, 2\}$. We verify that, as n increases, Z tends to different limit values that increase with β. In other words, when n is large, Z is affected only by p and R, as given in expression (44). In fact, β is proportional to z_L, and based on the relation between b and z_L, b is also proportional to β. According to (22), p increases with β, leading to the increase of Z for fixed values of R. In addition, we observe that for large values, the effect of β on Z becomes weaker.

We now vary β and R, while fixing $n = 50$ and maintaining the other parameters. Fig. 8 shows the evolution of Z versus $\beta \in [0, 2]$, for $R \in \{0.1, 0.3, 0.5, 1\}$. The value of Z gradually increases with β, reaching limit values that increase with R. At the same time, we can see that the effect of R on the impedance between the points a and c is smaller as R decreases. Moreover, β can vary within a large range (as shown in Fig. 7 when $R = 0.1$), showing that the fractional order inductance can have high influence on the impedance.

Finally, we vary β and L, while keeping the values of the other parameters. Fig. 9 shows the evolution of Z versus $\beta \in [0, 2]$, for $L \in \{0.01, 0.03, 0.05, 0.1\}$. We verify that, for large values of β, the magnitude of the impedance Z tends to the same value, independently of L. This is explained by the fact that p in (44) does not vary in this case. Therefore, the effect of β can either be increased or decreased to meet the requirements of any practical application, which is not possible with traditional integer-order ECN.

From Figs. 8 and 9, we verify that when the FO parameter β is small, L plays a major role in Z. On the contrary, when β is large, R plays a leading role. This behavior is not observed in integer-order ECN.

4.2. Magnitude characteristics of the impedance between points c and f

We chose $R = 0.1, L = 0.01, C = 1, \omega = 300$ and we vary the number of units n and the FO values α and β. Figs. 10 and 11 depict the evolution of Z versus $n \in [0, 50]$ and $\alpha \in \{0.1, 0.4, 0.7, 1, 2\}$ for $\beta = 1$, and versus $n \in [0, 50]$ and $\beta \in \{0.1, 0.4, 0.7, 1, 2\}$ for $\alpha = 1$, respectively. We verify that, for any values of α and β, the magnitude of the impedance Z varies with n, increasing linearly for fixed values of α and non linearly for fixed values of β.

The impedance analysis between the points c and d is omitted here, since comparing expressions (59) and (68), we verify that the two impedances are similar.

4.3. Relationship between the impedance magnitude and the fractional-order

From Figs. 10 and 11, we also verify that the influence of the number of units n on Z diminishes as α and β increase. In the limit, namely for $\alpha, \beta = 2$, the effect on Z is minimal. This is consistent with the results in Figs. 12–17, that depict Z between the points c and f for different parameter combinations, with $\omega = 300$ and $n = 50$.

Fig. 12 represents Z versus $R \in \{0.1, 0.2, 0.4, 0.6, 0.8, 1\}$ and $\beta \in [0, 2]$, for $L = 0.01, C = 1$ and $\alpha = 1$. For a given β, the magnitude of the impedance increases with R, approaching distinct limit values as β increases. Meanwhile, one can observe that the effect of R on the impedance between the points c and f is smaller as the value of R decreases. This is an effect similar to the one depicted in Fig. 8. Fig. 13 depicts Z versus $\alpha \in [0, 2]$,

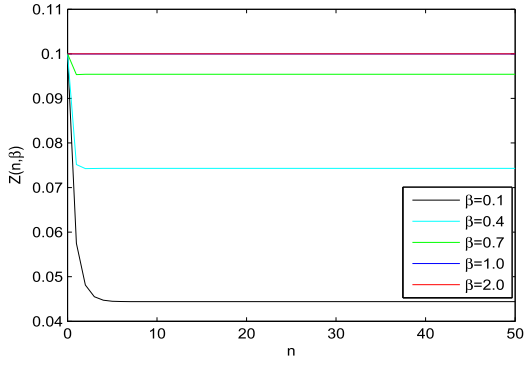

Fig. 7 The magnitude of the impedance, Z, of the FO-ECN between the points a and c versus $n \in [0, 50]$ and $\beta \in \{0.1, 0.4, 0.7, 1, 2\}$, for $R = 0.1, L = 0.01$ and $\omega = 300$.

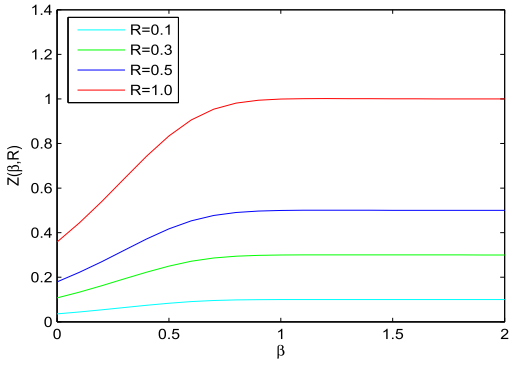

Fig. 8 The magnitude of the impedance, Z, of the FO-ECN between the points a and c versus $\beta \in [0, 2]$ and $R \in \{0.1, 0.3, 0.5, 1\}$, for $L = 0.01, \omega = 300$ and $n = 50$.

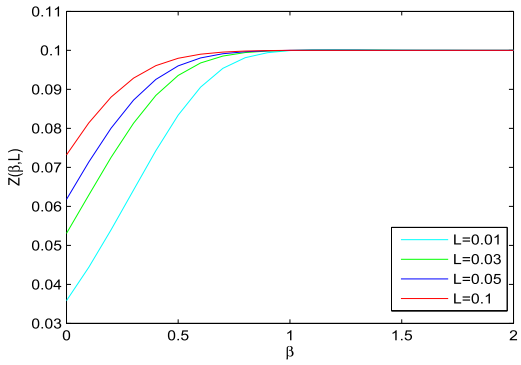

Fig. 9 The magnitude of the impedance, Z, of the FO-ECN between the points a and c versus $\beta \in [0, 2]$ and $L \in \{0.01, 0.03, 0.05, 0.1\}$, for $R = 0.1, \omega = 300$ and $n = 50$.

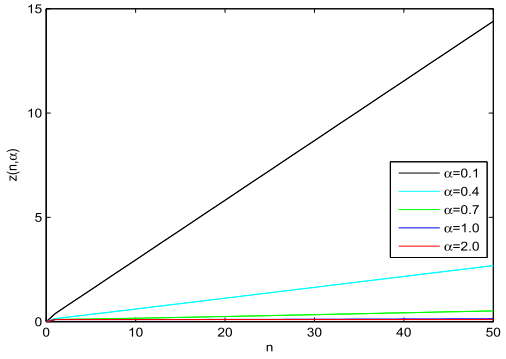

Fig. 10 The magnitude of the impedance, Z, of the FO-ECN between the points c and f versus $n \in [0, 50]$ and $\alpha \in \{0.1, 0.4, 0.7, 1, 2\}$, for $R = 0.1, L = 0.01, C = 1, \omega = 300$ and $\beta = 1$.

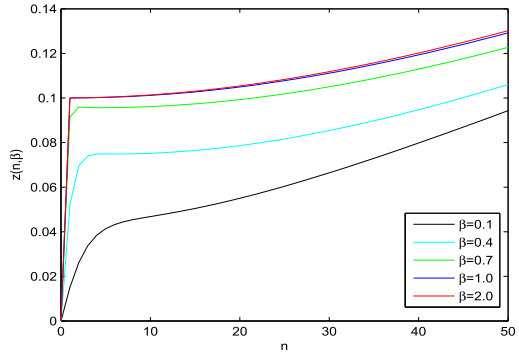

Fig. 11 The magnitude of the impedance, Z, of the FO-ECN between the points c and f versus $n \in [0, 50]$ and $\beta \in \{0.1, 0.4, 0.7, 1, 2\}$, for $R = 0.1, L = 0.01, C = 1, \omega = 300$ and $\alpha = 1$.

while $\beta = 1$ and maintaining the rest of the parameters. As α increases, Z decays rapidly to a stable value close to 0. Comparing Figs. 12 and 13, we verify that for obtaining a small Z, we only need to choose a small R. This corresponds to a reduced power loss in the FO-ECN. Fig. 14 depicts the evolution of Z versus $\beta \in [0, 2]$ and $L \in \{0.01, 0.02, 0.04, 0.06, 0.08, 0.1\}$, for $R = 0.1, C = 1$ and $\alpha = 1$. The magnitude of the impedance Z converges to the value $Z = 0.13$ as β increases, independently of L. This agrees with expression (59). Meanwhile, for large values of β, the magnitude of the impedance Z tends to the same value, independently of L (similarly to the effect observed in with Fig. 9). Fig. 15 shows Z versus $\alpha \in [0, 2]$ for $\beta = 1$ and maintaining the values of the other parameters. We note that the value of L has little effect on Z and that Z decays rapidly to values nearly 0 when α increases.If we want to adjust the value of L, then α can take any value within the interval $[0 - 2]$ and will not affect the Z. This shows that the choice of the fractional order capacitor can have a considerable freedom. Figs. 16 and 17 depict the effect of $C \in \{1, 2, 4, 6, 8, 10\}$ for $\alpha = 1$ with $\beta \in [0, 2]$, and for $\beta = 1$ with $\alpha \in [0, 2]$, respectively, when $R = 0.1$ and $L = 0.01$. Independently of C, the magnitude of the impedance Z increases with β and decreases with α, reaching stable values. Moreover, the influence of C on Z becomes smaller as C increases. Large values of Z can be obtained by choosing small values of α. The relationship between Z and the parameters (R, L, C, n) depends on the orders β and α. Therefore, in practical applications, if we need large, or small, values of Z, then we can adjust β and α. This behavior emphasizes the flexibility of the FO-ECN.

5. Validity of the derivation

The impedance equations of the FO-ECN were derived for three different cases, using matrix transformation and constructing differential equations. In the follow-up, we compare our results with those obtained with the conventional equivalent resistance calculation method.

We verify the accuracy of the equivalent impedance formula between the two points a and c derived in Section 3. Similarly, the equivalent impedance equation between the points c and f, or c and d, can also be verified by using the equipotential method and the $Y - \triangle$ transformation. Due to space constraints, they will be omitted here.

Based on the symmetry of the FO-ECN, we have $I_{bn} = 0$, meaning there is no current flows through the fractional capacitance in the circuit. Therefore, according to this property, we simplify the circuit diagram, and the circuit diagram when $n = \{1, 2, 3\}$ is shown in Figs. 18–20.

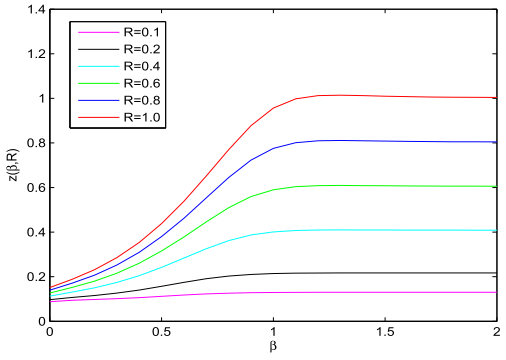

Fig. 12 The magnitude of the impedance, Z, of the FO-ECN between the two points c and f versus $\beta \in [0, 2]$ and $R \in \{0.1, 0.2, 0.4, 0.6, 0.8, 1\}$, for $L = 0.01, C = 1, \omega = 300, n = 50$ and $\alpha = 1$.

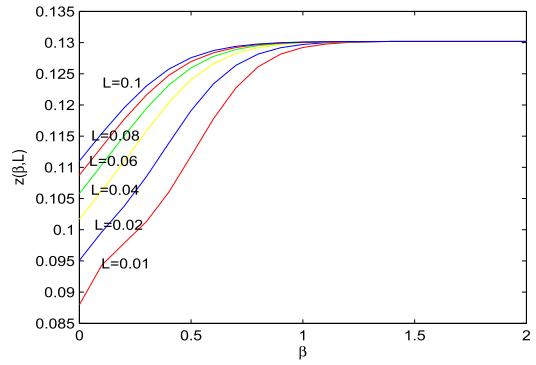

Fig. 13 The magnitude of the impedance, Z, of the FO-ECN between the two points c and f versus $\alpha \in [0,2]$ and $R \in \{0.1, 0.2, 0.4, 0.6, 0.8, 1\}$, for $L = 0.01, C = 1, \omega = 300, n = 50$ and $\beta = 1$.

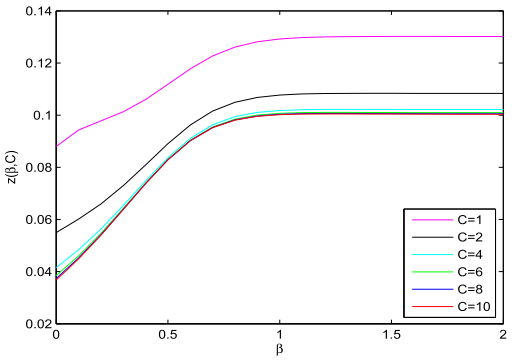

Fig. 16 The magnitude of the impedance, Z, of the FO-ECN between the two points c and f versus $\beta \in [0,2]$ and $C \in \{1, 2, 4, 6, 8, 10\}$, for $R = 0.1, L = 0.01, \omega = 300, n = 50$ and $\alpha = 1$.

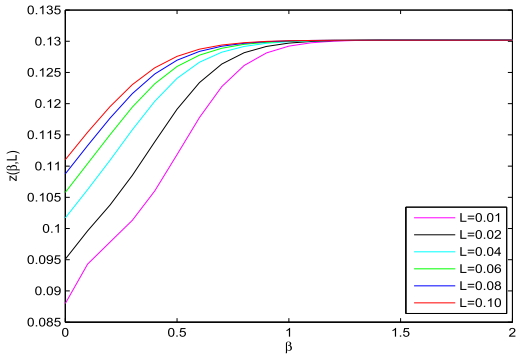

Fig. 14 The magnitude of the impedance, Z, of the FO-ECN between the two points c and f versus $\beta \in [0,2]$ and $L \in \{0.01, 0.02, 0.04, 0.06, 0.08, 0.1\}$, for $R = 0.1, C = 1, \omega = 300$, $n = 50$ and $\alpha = 1$.

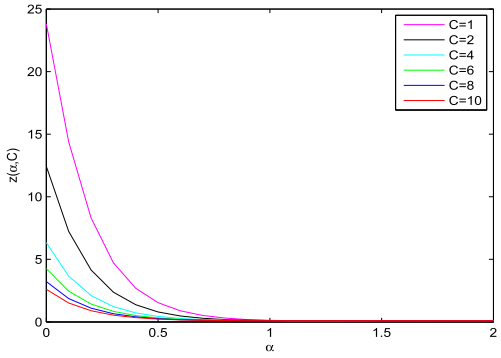

Fig. 17 The magnitude of the impedance, Z, of the FO-ECN between the two points c and f versus $\alpha \in [0,2]$ and $C \in \{1, 2, 4, 6, 8, 10\}$, for $R = 0.1, L = 0.01, \omega = 300, n = 50$ and $\beta = 1$.

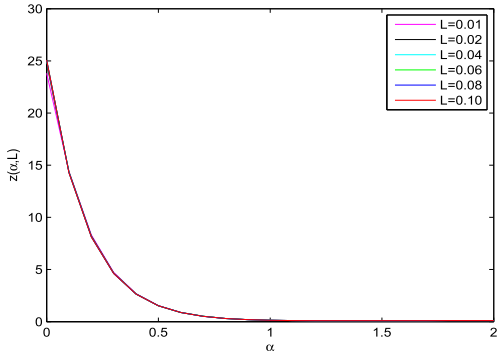

Fig. 15 The magnitude of the impedance, Z, of the FO-ECN between the two points c and f versus $\alpha \in [0,2]$ and $L \in \{0.01, 0.02, 0.04, 0.06, 0.08, 0.1\}$, for $R = 0.1, C = 1, \omega = 300$, $n = 50$ and $\beta = 1$.

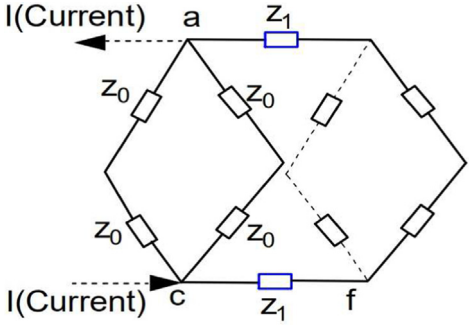

Fig. 18 Circuit diagrams of the circuit network between a and c at $n = 1$.

According to the equipotential method and the calculation formula of series and parallel resistances, from Fig. 7 we get:

$$Z_{ac}(1) = \frac{z_0^2 + 2z_0z_1}{2z_0 + 2z_1}. \tag{69}$$

Similarly, from Figs. 8 and 9, we obtain:

$$Z_{ac}(2) = \frac{z_0^3 + 4z_0z_1^2 + 6z_0^2z_1}{3z_0^2 + 4z_1^2 + 8z_0z_1}, \tag{70}$$

$$Z_{ac}(3) = \frac{z_0^4 + 12z_0^3z_1 + 8z_0z_1^3 + 16z_0z_1^2 + 4z_0^2z_1^2}{4z_0^3 + 8z_1^3 + 16z_1^2 + 8z_0z_1^2 + 8z_0z_1 + 12z_0^2z_1}. \tag{71}$$

From expression (42), it yields:

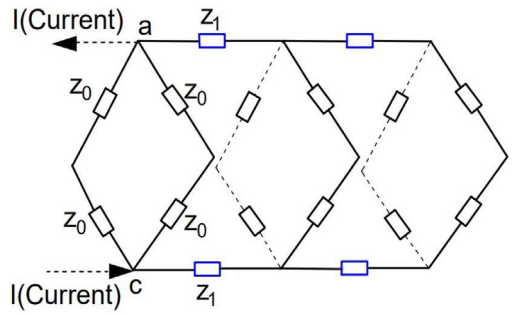

Fig. 19 Circuit diagrams of the circuit network between a and c at $n = 2$.

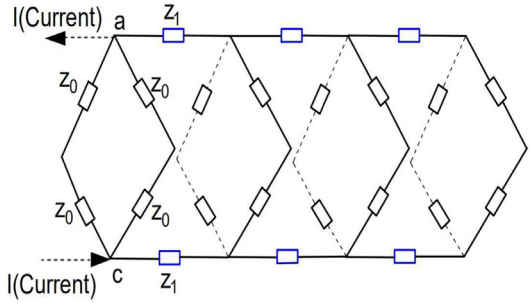

Fig. 20 Circuit diagrams of the circuit network between a and c at $n = 3$.

$$Z_{ac}(1) = \left(1 - \frac{p-q}{p^2-q^2}\right) z_0, \tag{72}$$

$$Z_{ac}(2) = \left(1 - \frac{p^2-q^2}{p^3-q^3}\right) z_0, \tag{73}$$

$$Z_{ac}(3) = \left(1 - \frac{p^3-q^3}{p^4-q^4}\right) z_0. \tag{74}$$

The numerical values (i) $z_0 = 1, z_1 = 0.01$, (ii) $z_0 = 0.5, z_1 = 0.01$, (iii) $z_0 = 1, z_1 = 0.1$ were substituted into Eqs. (69)–(71) Eqs. (72)–(74) for numerical verification and the results are listed in Table 1. We verify that the results are identical for the three different sets of z_0 and z_1, when using the previous method and the formulas derived in Section 3.1. Additionally, the accuracy and validity of the impedance equation derived in this paper is confirmed.

6. Phase characteristics of the impedance

In this section, we investigate the relationship between the impedance phase and the FO, under different values of the parameters R, L, C and ω.

6.1. Phase characteristics between the points a and c

We now select $\alpha = 1, n = 50$ and $\beta \in [0, 2]$. Fig. 21 depicts the impedance phase, ϕ, versus β and $R \in \{0.1, 0.4, 0.7, 1\}$, for $L = 0.01$ and $\omega = 300$. Fig. 22 shows ϕ versus β and $L \in \{0.01, 0.04, 0.07, 0.1\}$, for $R = 0.1$ and $\omega = 300$. Fig. 23 presents ϕ versus β and $\omega \in \{100, 200, 300, 400\}$, for $R = 0.1$

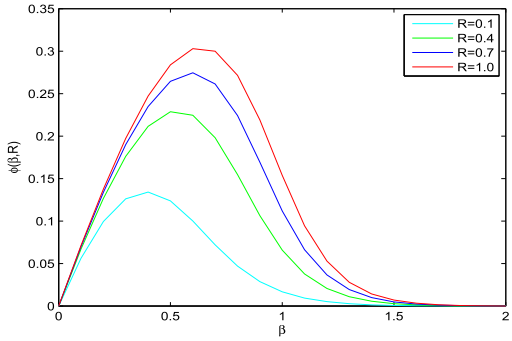

Fig. 21 The phase of the impedance, ϕ, between the points a and c versus $\beta \in [0, 2]$ and $R \in \{0.1, 0.4, 0.7, 1\}$, for $L = 0.01, \omega = 300$ and $n = 50$.

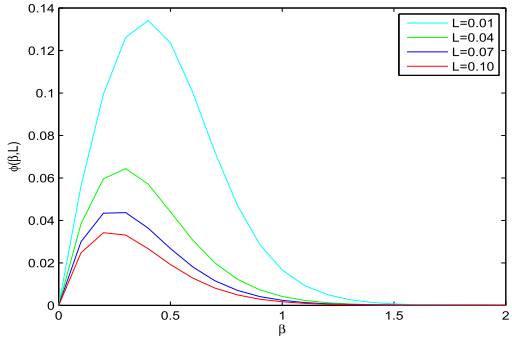

Fig. 22 The phase of the impedance, ϕ, between the points a and c versus $\beta \in [0, 2]$ and $L \in \{0.01, 0.04, 0.07, 0.1\}$, for $R = 0.1, \omega = 300$ and $n = 50$.

Table 1 Verification of the accuracy and validity of the equivalent impedance formula between two points a and c

Computing method	Formula	$z_0 = 1, z_1 = 0.01$	$z_0 = 0.5, z_1 = 0.01$	$z_0 = 1, z_1 = 0.1$
Previous method	Z_{ac}(i) in (69)	0.5050	0.2549	0.5455
	Z_{ac}(ii) in (70)	0.3442	0.1774	0.4271
	Z_{ac}(iii) in (71)	0.2670	0.1415	0.3854
Proposed method	Z_{ac}(i) in (72)	0.5050	0.2549	0.5455
	Z_{ac}(ii) in (73)	0.3442	0.1774	0.4271
	Z_{ac}(iii) in (74)	0.2670	0.1415	0.3854

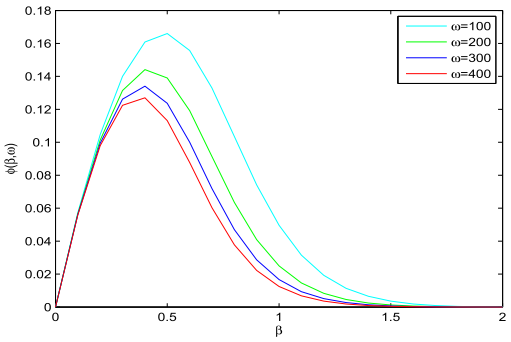

Fig. 23 The phase of the impedance, ϕ, between the points a and c versus $\beta \in [0,2]$ and $\omega \in \{100,200,300,400\}$, for $R = 0.1, L = 0.01$ and $n = 50$.

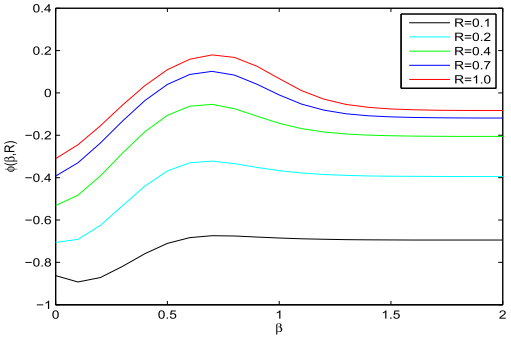

Fig. 24 The phase of the impedance, ϕ, between the points c and f versus $\beta \in [0,2]$ and $R \in \{0.1,0.2,0.4,0.7,1\}$, for $L = 0.01, C = 1, \omega = 300, n = 50$ and $\alpha = 1$.

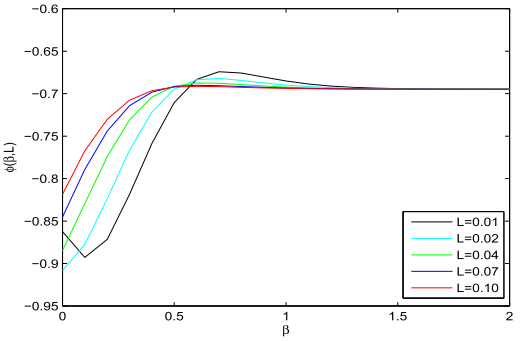

Fig. 25 The phase of the impedance, ϕ, between the points c and f versus $\beta \in [0,2]$ and $L \in \{0.01,0.02,0.04,0.07,0.1\}$, for $R = 0.1, C = 1, \omega = 300, n = 50$ and $\alpha = 1$.

and $L = 0.01$. We verify that as β increases, ϕ gives a leading angle that increases to a maximum and then decreases to values close to 0. The maxima are obtained for $R = 1.0, L = 0.001$ and $\omega = 100$, respectively. Moreover, it can be seen that the leading angle increases with R and decreases with L and ω.

6.2. Phase characteristics of the impedance between the points c and f

In this case, we maintain the values of $\alpha = 1, n = 50$ and $\beta \in [0,2]$. Fig. 24 depicts ϕ versus β and

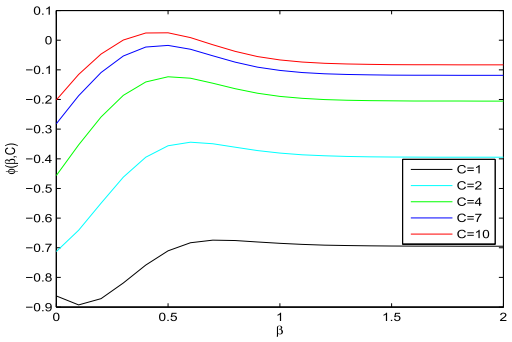

Fig. 26 The phase of the impedance, ϕ, between the points c and f versus $\beta \in [0,2]$ and $C \in \{1,2,4,7,10\}$, for $R = 0.1, L = 0.01, \omega = 300, n = 50$ and $\alpha = 1$.

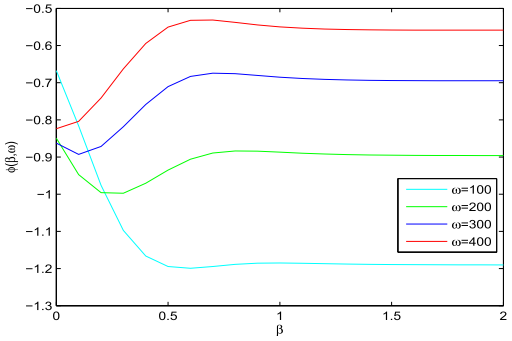

Fig. 27 The phase of the impedance, ϕ, between the points c and f versus $\beta \in [0,2]$ and $\omega \in \{100,200,300,400\}$, for $R = 0.1, L = 0.01$ and $C = 1, n = 50$ and $\alpha = 1$.

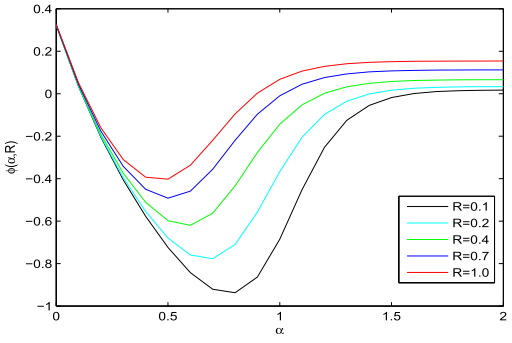

Fig. 28 The phase of the impedance between the points c and f versus $\alpha \in [0,2]$ and $R \in \{0.1,0.2,0.4,0.7,1\}$, for $L = 0.01, C = 1, \omega = 300, n = 50$ and $\beta = 1$.

$R \in \{0.1,0.2,0.4,0.7,1\}$, for $L = 0.01, C = 1$ and $\omega = 300$. Fig. 25 shows ϕ versus β and $L \in \{0.01,0.04,0.07,0.1\}$, for $R = 0.1, C = 1$ and $\omega = 300$. Fig. 26 illustrates the evolution of ϕ versus β and $C \in \{1,2,4,7,10\}$, for $R = 0.1, L = 0.01$ and $\omega = 300$. Fig. 27 represents ϕ versus β and $\omega \in \{100,200,300,400\}$, for $R = 0.1, L = 0.01$ and $C = 1$. We note in Figs. 24 and 26 that ϕ changes from lag to lead, while in Figs. 25 and 27 the angle ϕ corresponds always to a lag. Moreover, the lag angle decreases with the increase of R, L, C and ω. When $\omega = 100$ and $L = 0.01$, the phase angle first decreases and then increases with β, revealing a particular behavior, as shown in Figs. 25 and 27.

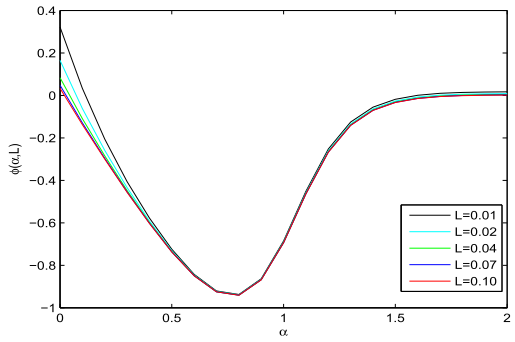

Fig. 29 The phase of the impedance between the points c and f versus $\alpha \in [0,2]$ and $L \in \{0.01, 0.02, 0.04, 0.07, 0.1\}$, for $R = 0.1, C = 1, \omega = 300, n = 50$ and $\beta = 1$.

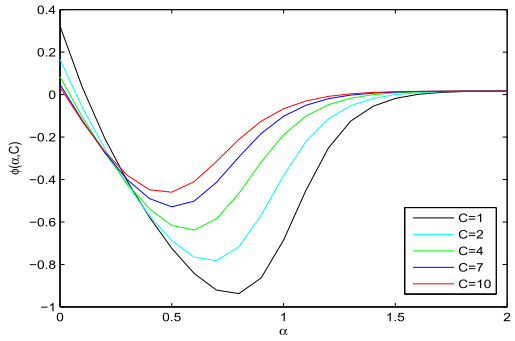

Fig. 30 The phase of the impedance between the points c and f versus $\alpha \in [0,2]$ and $C \in \{1, 2, 4, 7, 10\}$, for $R = 0.1, L = 0.01, \omega = 300, n = 50$ and $\beta = 1$.

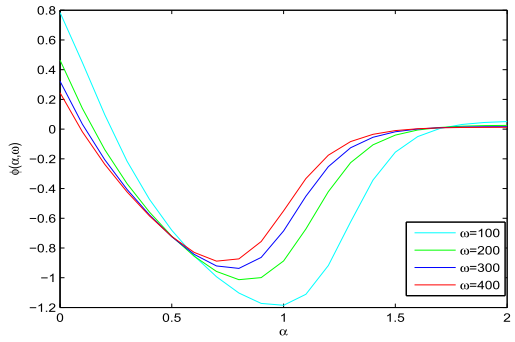

Fig. 31 The phase of the impedance between the points c and f versus $\alpha \in [0,2]$ and $\omega \in \{100, 200, 300, 400\}$, for $R = 0.1, L = 0.01$ and $C = 1, n = 50$ and $\beta = 1$.

We now select $\beta = 1$ and $\alpha \in [0,2]$, while maintaining the remaining parameters. Figs. 28–31 show ϕ versus α for various values of R, L, C and ω. We verify that, as α increases, the lag angle ϕ first increases to a maximum and then decreases reaching a limit value. Moreover, the lag angle ϕ increases with R, C and ω, and remains almost unaffected by L.

6.3. Comparative analysis

Let us denote by $\phi(ac)$ and $\phi(cf)$ the phase of the impedance between the points a and c, and c and f, respectively. Figs. 32–34 depict the relation between $\phi(ac)$ and $\phi(cf)$, and the param-

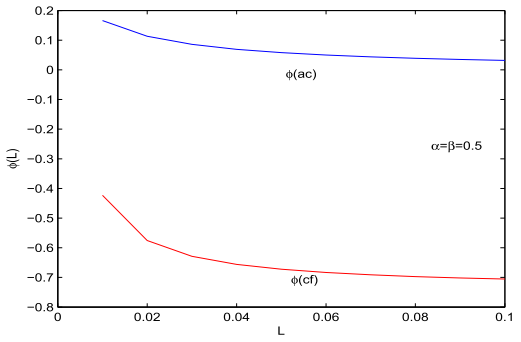

Fig. 32 Variation of $\phi(ac)$ and $\phi(cf)$ versus $L \in [0, 0.1]$, for $\alpha = \beta = 0.5$.

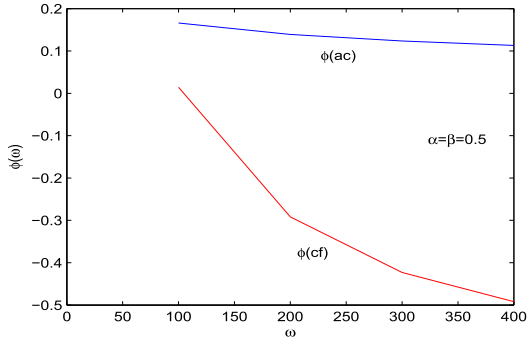

Fig. 33 Variation of $\phi(ac)$ and $\phi(cf)$ versus $\omega \in [0, 400]$, for $\alpha = \beta = 0.5$.

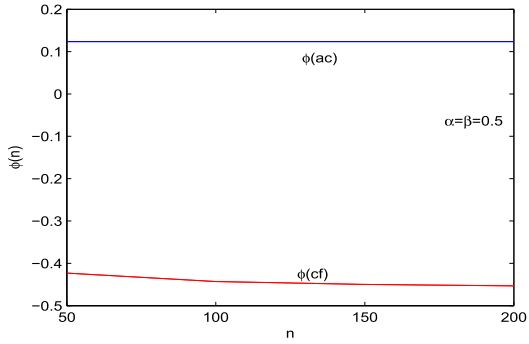

Fig. 34 Variation of $\phi(ac)$ and $\phi(cf)$ versus $n \in [50, 200]$, for $\alpha = \beta = 0.5$.

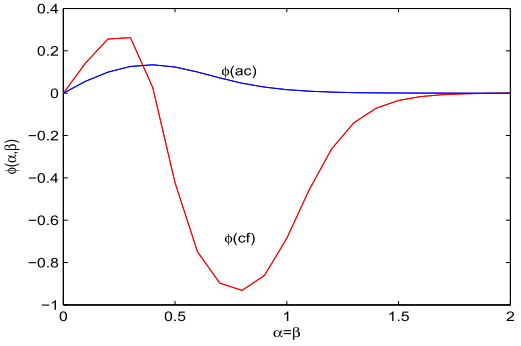

Fig. 35 Variation of $\phi(ac)$ and $\phi(cf)$ versus $\alpha, \beta \in [0, 2]$, for $\alpha = \beta$.

eters L, C and n, respectively. We verify that $\phi(cf)$ is a lag angle that increases with L, ω and n. On the other hand, $\phi(ac)$ is a lead angle that decreases with L and ω, and is not affected by n.

Fig. 35 depicts the variation of $\phi(ac)$ and $\phi(cf)$ versus $\alpha, \beta \in [0, 2]$, for $\alpha = \beta, \omega = 300, R = 0.1, C = 1, L = 0.01$ and $n = 50$. We notice that $\phi(ac)$ is a lead angle that firstly increases and then decreases with α and β. On the other hand, $\phi(cf)$ is firstly a lead angle and then changes to lag, when α and β increase. In both cases the evolution is smooth with lead and lag peaks.

7. Conclusion

This paper introduced the modeling and analysis of a class of $\diamondsuit \times n$ RLC FO-ECN. First, an equivalent circuit network model was established. Then, using the Kirchhoff's laws, a recursive relation of the equivalent resistance was found. Finally, three general models for the impedances between two nodes of the FO-ECN were derived. The effect of the FO-ECN parameters $R, L, C, n, \beta, \alpha$ and ω on the impedance magnitude and phase characteristics were studied. The results show that the characteristics of complex FO-ECN are different from those of the integer-order resistance network. Moreover, some new dynamical phenomena not observed in classical integer-order ECN were unraveled. These characteristics are relevant since having more flexibility to the design of ECN. Therefore, it is possible to use the derived formulas to design and analyze the ECN in practical applications. Carrying out laboratory experiments to illustrate the results of theoretical and numerical analysis is the work to be developed in the follow-up of this study.

Declaration of Competing Interest

The authors declare that they have no known competing financial interests or personal relationships that could have appeared to influence the work reported in this paper.

Acknowledgments

This work was supported by the National Natural Science Funds of China (No. 11971032).

Appendix A. The fractional impedance of inductors and capacitors is given by:

$$\begin{aligned} Z_L(s) &= s^{\beta} L, \\ Z_C(s) &= \tfrac{1}{s^{\alpha} C}. \end{aligned}$$

By substituting $s = j\omega$ in Z_L and Z_C, the frequency-dependent impedance is given as follow:

$$\begin{aligned} Z_L(j\omega) &= (j\omega)^{\beta} L = j^{\beta}\omega^{\beta} L, \\ Z_C(j\omega) &= \tfrac{1}{(j\omega)^{\alpha} C} = \tfrac{1}{j^{\alpha}\omega^{\alpha} C} = \tfrac{j^{-\alpha}}{\omega^{\alpha} C}, \end{aligned}$$

Taking the logarithm on both sides of the Euler formula $e^{jx} = \cos x + j \sin x$, one can get:

$$jx = \ln(\cos x + j \sin x),$$

For $x = \frac{\pi}{2}$, it yields

$$\frac{\pi}{2} j = \ln(j),$$

Then one can obtain

$$j = e^{\frac{\pi}{2} j},$$

so that

$$\begin{aligned} j^{\beta} &= e^{\frac{\beta\pi}{2} j}, \\ j^{-\alpha} &= e^{\frac{-\alpha\pi}{2} j}. \end{aligned}$$

Substituting the above two formulas into Z_L and Z_C, one has

$$\begin{aligned} Z_L(j\omega) &= j^{\beta}\omega^{\beta} L = e^{\frac{\beta\pi}{2} j}\omega^{\beta} L, \\ Z_C(j\omega) &= \tfrac{j^{-\alpha}}{\omega^{\alpha} C} = \tfrac{e^{\frac{-\alpha\pi}{2} j}}{\omega^{\alpha} C}. \end{aligned}$$

It follows from Euler's formula $e^{jx} = \cos x + j \sin x$ that

$$\begin{aligned} Z_L(j\omega) &= \omega^{\beta} L \cos\left(\tfrac{\beta\pi}{2}\right) + j\omega^{\beta} L \sin\left(\tfrac{\beta\pi}{2}\right), \\ Z_C(j\omega) &= \tfrac{\cos\left(\frac{\alpha\pi}{2}\right)}{\omega^{\alpha} C} - j\tfrac{\sin\left(\frac{\alpha\pi}{2}\right)}{\omega^{\alpha} C}. \end{aligned}$$

References

[1] J.T. Machado, A.M. Lopes, Fractional-order modeling of a diode, Commun. Nonlinear Sci. Numer. Simul. 70 (2019) 343–353.

[2] J.T. Machado, Fractional order junctions, Commun. Nonlinear Sci. Numer. Simul. 20 (1) (2015) 1–8.

[3] J.T. Machado, Matrix fractional systems, Commun. Nonlinear Sci. Numer. Simul. 25 (1–3) (2015) 10–18.

[4] K.S. Miller, B. Ross, An Introduction to Fractional Calculus and Fractional Differential Equations, Wiley, New York.

[5] K. Xu, L. Chen, M. Wang, A.M. Lopes, J. Tenreiro Machado, H. Zhai, Improved decentralized fractional PD control of structure vibrations, Mathematics 8 (3) (2020) 326.

[6] L. Chen, H. Yin, T. Huang, L. Yuan, S. Zheng, L. Yin, Chaos in fractional-order discrete neural networks with application to image encryption, Neural Netw.: Off. J. Int. Neural Netw. Soc. 125 (2020) 174–184.

[7] L. Chen, R. Wu, Y. He, L. Yin, Robust stability and stabilization of fractional-order linear systems with polytopic uncertainties, Appl. Math. Comput. 257 (2015) 274–284.

[8] L. Chen, T. Huang, J.T. Machado, A.M. Lopes, Y. Chai, R. Wu, Delay-dependent criterion for asymptotic stability of a class of fractional-order memristive neural networks with time-varying delays, Neural Netw. 118 (2019) 289–299.

[9] L. Chen, T. Huang, J.T. Machado, A.M. Lopes, Y. Chai, R. Wu, Delay-dependent criterion for asymptotic stability of a class of fractional-order memristive neural networks with time-varying delays, Neural Netw. 118 (2019) 289–299.

[10] X.-J. Yang, New rheological problems involving general fractional derivatives with nonsingular power-law kernels, Proc. Romanian Acad. Ser. A-Math. Phys. Tech. Sci. Inf. Sci. 19 (1) (2018) 45–52.

[11] X.-J. Yang et al, New general fractional-order rheological models with kernels of Mittag-Leffler functions, Rom. Rep. Phys. 69 (4) (2017) 118.

[12] X.-J. Yang, F. Gao, J.T. Machado, D. Baleanu, A new fractional derivative involving the normalized sinc function without singular kernel, Eur. Phys. J. Special Top. 226 (16–18) (2017) 3567–3575.

[13] X.-J. Yang, F. Gao, H. Srivastava, A new computational approach for solving nonlinear local fractional PDEs, J. Comput. Appl. Math. 339 (2018) 285–296.

[14] X.-J. Yang, F. Gao, H. Srivastava, Non-differentiable exact solutions for the nonlinear ODEs defined on fractal sets, Fractals 25 (04) (2017) 1740002.

[15] X.-J. Yang, J. Machado, J.J. Nieto, A new family of the local fractional PDEs, Fundamenta Informaticae 151 (1–4) (2017) 63–75.
[16] W. Gao, P. Veeresha, D. Prakasha, H.M. Baskonus, G. Yel, A powerful approach for fractional Drinfeld–Sokolov–Wilson equation with Mittag-Leffler law, Alexandria Eng. J. 58 (4) (2019) 1301–1311.
[17] W. Gao, M. Partohaghighi, H.M. Baskonus, S. Ghavi, Regarding the group preserving scheme and method of line to the numerical simulations of Klein-Gordon model, Res. Phys. 15 (2019) 102555.
[18] H. Baskonus, J. Gómez-Aguilar, New singular soliton solutions to the longitudinal wave equation in a magneto-electro-elastic circular rod with m-derivative, Mod. Phys. Lett. B 33 (21) (2019) 1950251.
[19] H.M. Baskonus, Complex surfaces to the fractional $(2+1)$-dimensional boussinesq dynamical model with the local M-derivative, Eur. Phys. J. Plus 134 (7) (2019) 322.
[20] D. Prakasha, P. Veeresha, H.M. Baskonus, Two novel computational techniques for fractional Gardner and Cahn-Hilliard equations, Comput. Math. Meth. 1 (2) (2019) e1021.
[21] A. Ciancio, A. Quartarone, A hybrid model for tumor-immune competition, UPB Sci. Bull. Ser. A 75 (4) (2013) 125–136.
[22] A. Ciancio, Analysis of time series with wavelets, Int. J. Wavelets Multiresolut. Inf. Process. 5 (02) (2007) 241–256.
[23] K. Biswas, G. Bohannan, R. Caponetto, A.M. Lopes, J.A.T. Machado, Fractional-order Devices, Springer, 2017.
[24] S. Westerlund, L. Ekstam, Capacitor theory, IEEE Trans. Dielectr. Electr. Insul. 1 (5) (1994) 826–839.
[25] F. Gómez, J. Rosales, M. Guía, RLC electrical circuit of non-integer order, Open Phys. 11 (10) (2013) 1361–1365.
[26] J. Gómez-Aguilar, V. Morales-Delgado, M. Taneco-Hernández, D. Baleanu, R. Escobar-Jiménez, M. Al Qurashi, Analytical solutions of the electrical RLC circuit via Liouville-Caputo operators with local and non-local kernels, Entropy 18 (8) (2016) 402.
[27] J. Gómez-Aguilar, T. Córdova-Fraga, J. Escalante-Martínez, C. Calderón-Ramón, R. Escobar-Jiménez, Electrical circuits described by a fractional derivative with regular kernel, Revista mMxicana de Física 62 (2) (2016) 144–154.
[28] J. Gómez-Aguilar, H. Yépez-Martínez, R. Escobar-Jiménez, C. Astorga-Zaragoza, J. Reyes-Reyes, Analytical and numerical solutions of electrical circuits described by fractional derivatives, Appl. Math. Model. 40 (21–22) (2016) 9079–9094.
[29] S. Kapoulea, G. Tsirimokou, C. Psychalinos, A.S. Elwakil, Generalized fully adjustable structure for emulating fractional-order capacitors and inductors of orders less than two, Circuits Syst. Signal Process. 39 (4) (2020) 1797–1814.
[30] A. Allagui, D. Zhang, I. Khakpour, A.S. Elwakil, C. Wang, Quantification of memory in fractional-order capacitors, J. Phys. D: Appl. Phys. 53 (2) (2019) 02LT03.
[31] S. Kapoulea, C. Psychalinos, A.S. Elwakil, A.G. Radwan, One-terminal electronically controlled fractional-order capacitor and inductor emulator, AEU-Int. J. Electron. Commun. 103 (2019) 32–45.
[32] A.G. Radwan, A. Soliman, A.S. Elwakil, A. Sedeek, On the stability of linear systems with fractional-order elements, Chaos Solit. Fract. 40 (5) (2009) 2317–2328.
[33] M.S. Semary, M.E. Fouda, H.N. Hassan, A.G. Radwan, Realization of fractional-order capacitor based on passive symmetric network, J. Adv. Res. 18 (2019) 147–159.
[34] Y. Jiang, B. Zhang, High-power fractional-order capacitor with based on power converter, IEEE Trans. Industr. Electron. 65 (4) (2017) 3157–3164.
[35] G. Tsirimokou, C. Psychalinos, A. Elwakil, K. Salama, Experimental verification of on-chip CMOS fractional-order capacitor emulators, Electron. Lett. 52 (15) (2016) 1298–1300.
[36] M.C. Tripathy, D. Mondal, K. Biswas, S. Sen, Experimental studies on realization of fractional inductors and fractional-order bandpass filters, Int. J. Circuit Theory Appl. 43 (9) (2015) 1183–1196.
[37] J.F. Gomez-Aguilar, R.F. Escobar-Jimenez, M.G. Lopez-Lopez, V.M. Alvarado-Martinez, Atangana-Baleanu fractional derivative applied to electromagnetic waves in dielectric media, J. Electromagn. Waves Appl. 30 (15) (2016) 1937–1952.
[38] J.T. Machado, A.M. Galhano, Fractional order inductive phenomena based on the skin effect, Nonlinear Dyn. 68 (1–2) (2012) 107–115.
[39] Y. Hong, Z. Shuai, H. Cheng, C. Tu, Y. Li, Z.J. Shen, Stability analysis of low-frequency oscillation in train-network system using RLC circuit model, IEEE Trans. Transp. Electrification 5 (2) (2019) 502–514.
[40] K. Shringarpure, S. Pan, J. Kim, J. Fan, B. Achkir, B. Archambeault, J.L. Drewniak, Sensitivity analysis of a circuit model for power distribution network in a multilayered printed circuit board, IEEE Trans. Electromagn. Compat. 59 (6) (2017) 1993–2001.
[41] D. Jeltsema, R. Ortega, J.M. Scherpen, On passivity and power-balance inequalities of nonlinear RLC circuits, IEEE Trans. Circuits Syst. I: Fundam. Theory Appl. 50 (9) (2003) 1174–1179.
[42] M. Owaidat, R. Hijjawi, J. Khalifeh, Network with two extra interstitial resistors, Int. J. Theor. Phys. 51 (10) (2012) 3152–3159.
[43] J.H. Asad, Analysis of infinite d-dimensional networks–capacitance between two adjacent nodes, J. Electrostat. 71 (4) (2013) 754–755.
[44] M. Owaidat, R. Hijjawi, J. Khalifeh, Interstitial single resistor in a network of resistors application of the lattice Green's function, J. Phys. A: Math. Theor. 43 (37) (2010) 375204.
[45] R. Zhou, D. Chen, H.H.C. Iu, C. Qi, Fractional-order $L^{\beta}C^{\alpha}$ infinite rectangle circuit network, IET Circuits Devices Syst. 10 (5) (2016) 383–393.
[46] H. Zheng, Q. Jing, C. Di-Yi, H.H. Iu, Fractional-order $L^{\beta}C^{\alpha}$ filter circuit network, Chin. Phys. B 24 (8) (2015) 080204.
[47] M. Ün, M. Ün, F.S. Kiziltaş, Analysis of fractional-order $2\times n$ RLC circuit network by mesh currents method, in: 2016 Medical Technologies National Congress (TIPTEKNO), IEEE, 2016, pp. 1–4.
[48] K. Zhou, D. Chen, X. Zhang, R. Zhou, H.H.-C. Iu, Fractional-order three-dimensional circuit network, IEEE Trans. Circuits Syst. I Regul. Pap. 62 (10) (2015) 2401–2410.
[49] L. Zhou, Z.-Z. Tan, Q.-H. Zhang, A fractional-order multifunctional n-step honeycomb RLC circuit network, Front. Inf. Technol. Electronic Eng. 18 (8) (2017) 1186–1196.
[50] A.G. Radwan, K.N. Salama, Fractional-order RC and RL circuits, Circuits Syst. Signal Process. 31 (6) (2012) 1901–1915.